LAWRENCE
LIVERMORE
NATIONAL
LABORATORY

LLNL-CONF-420042

Imaging System to Measure Kinetics of Material Cluster Ejection During Exit-Surface Damage Initiation and Growth in Fused Silica

R. N. Raman, R. A. Negres, S. G. Demos

November 11, 2009

Boulder Damage Symposium
Boulder, CO, United States
September 20, 2009 through September 23, 2009

Disclaimer

Imaging system to measure kinetics of material cluster ejection during exit-surface damage initiation and growth in fused silica

Rajesh N. Raman, Raluca A. Negres, Stavros G. Demos*
Lawrence Livermore National Laboratory, 7000 East Avenue, Livermore, CA, USA 94550

ABSTRACT

Laser-induced damage on the surface of optical components typically is manifested by the formation of microscopic craters that can ultimately degrade the optics performance characteristics. It is believed that the damage process is the result of the material exposure to high temperatures and pressures within a volume on the order of several cubic microns located just below the surface. The response of the material following initial localized energy deposition by the laser pulse, including the timeline of events and the individual processes involved during this timeline, is still largely unknown. In this work we introduce a time-resolved microscope system designed to enable a detailed investigation of the sequence of dynamic events involved during surface damage. To best capture individual aspects of the damage timeline, this system is employed in multiple imaging configurations (such as multi-view image acquisition at a single time point and multi-image acquisition at different time points of the same event) and offers sensitivity to phenomena at very early delay times. The capabilities of this system are demonstrated with preliminary results from the study of exit-surface damage in fused silica. The time-resolved images provide information on the material response immediately following laser energy deposition, the processes later involved during crater formation or growth, the material ejecta kinetics, and overall material motion and transformation. Such results offer insight into the mechanisms governing damage initiation and growth in the optical components of ICF class laser systems.

Keywords: Time-resolved imaging, microscopy, fused silica, surface damage initiation, damage growth

1. INTRODUCTION

1.1 Background

Laser-induced damage in the exit-surface in fused silica optics has been a topic of considerable study. Damage initiation sites are typically on the order of 10 μm in diameter, depending on the laser pulse length, but tend to grow exponentially under subsequent laser irradiation [1-5]. Microscopic examination of these sites reveals the formation of a damage crater containing modified material believed to be the result of exposure to high pressures and/or temperatures, as well as cleaved surfaces and cracks [6-9]. Although various models regarding the processes involved during a surface damage event have been proposed based on post-mortem examination of the crater characteristics for various laser parameters, there are only limited experimental studies that capture the dynamic processes during a damage event [10-12]. Of particular importance are experimental data on the laser-material interactions during the laser pulse that governs the energy deposition process. It is therefore apparent that an imaging system capable of capturing the material response through the timeline of events involved during surface damage would greatly enhance our understanding of the fundamental mechanisms involved.

1.2 System Requirements

To successfully capture all of the important processes during the damage timeline, such a time-resolved system must provide adequate spatial and temporal resolution to image the material changes and the dynamic events during damage initiation and growth. Specifically, this system must have the ability to measure lateral and depth dimensions of crater formation and growth, the onset and propagation of shock fronts, material transformations, and material kinetics at various delay times. In addition, this system must be able to accurately estimate particle (material ejecta) size, speed, trajectory, and time of ejection relative to the arrival of the damage pulse. Another requirement is to match the static spatial resolution (~1 μm) in the imaging of dynamic phenomena.

In this work, we describe a time-resolved microscope system specifically designed to meet the above requirements. This system is employed in various configurations in order to optimize its ability to detect and image the different processes

*demos1@llnl.gov; phone 1 925 423-3388

involved during the timeline. Experiments carried out using this system to study exit-surface damage in fused silica demonstrate its capabilities to capture the material modification and removal process through the entire damage timeline.

2. EXPERIMENTAL SYSTEM AND PRELIMINARY RESULTS

2.1 Sample and damage initiation protocol

The samples used in this study were circular fused silica optical flats having diameter of 50 mm and thickness of 10 mm. To simulate damage occurring under operating conditions relevant to large-aperture laser systems, the damaging (or *pump*) laser pulse must spatially overfill the initiated or growing damage sites, which can be on the order of 10 μm or 100 μm in diameter, respectively. To meet this requirement, a 150-mm focal length lens was used to focus the output of a pump laser (Quanta-Ray, Spectra-Physics) operating at 355 nm (3ω), 7-ns FWHM in duration, about 20 mm behind the exit-surface of the sample. In this arrangement, we estimate the pump beam diameter at the exit surface to be ~1 mm. Pristine surface sites were first exposed to an average fluence of ~30 J/cm^2 and damage initiation was observed with ~80% probability. This procedure leads to the formation of single or multi-pit craters with average pit diameter on the order of 10-50 μm. These sites were subsequently exposed to 3 or 4 additional laser pulses at a fluence of ~12 J/cm^2 which most often caused growth in the site's size (referred to as damage growth).

2.2 Time-resolved microscope system for imaging crater formation and material ejection

Since surface damage is associated with the formation of craters via material ejection, we initially designed our system to be able to capture this main process. Specifically, the system should be able to simultaneously record images that capture both the material ejection process as well as the formation of the damage site and its lateral dimensions at different time points as required. To achieve this capability, two microscope systems were employed with their image planes positioned parallel and perpendicular to the sample's surface. The corresponding images are referred to as the transmission-view (T-V) and side-view (S-V) images, respectively. Both microscopes were identical, utilizing a long working distance 5X objective (Mitutoyo, Japan) followed by a 5X zoom lens. The images were focused onto a CCD detector (Spiricon, 1616 pixels × 1216 pixels) with individual pixel size of 4.4 μm. The resulting spatial resolution was on the order of 1 μm. The focal planes of the two microscopes intersected at the sample's surface at the pump beam location. In this way, the damage sites formed in this volume were imaged with optimal spatial resolution by both microscopes. A schematic of this system configuration is provided in Fig. 1.

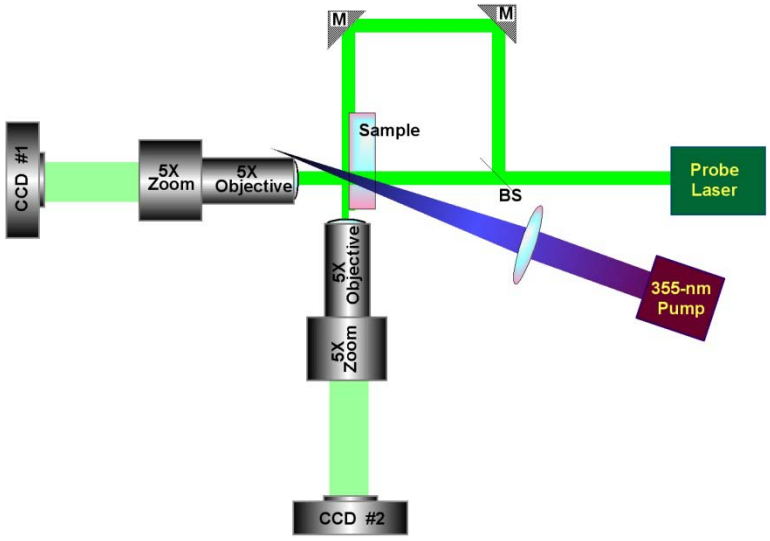

Figure 1. Basic time-resolved microscope system for simultaneous acquisition of transmission-view (T-V) and side-view (S-V) images of surface damage sites at various points during the timeline.

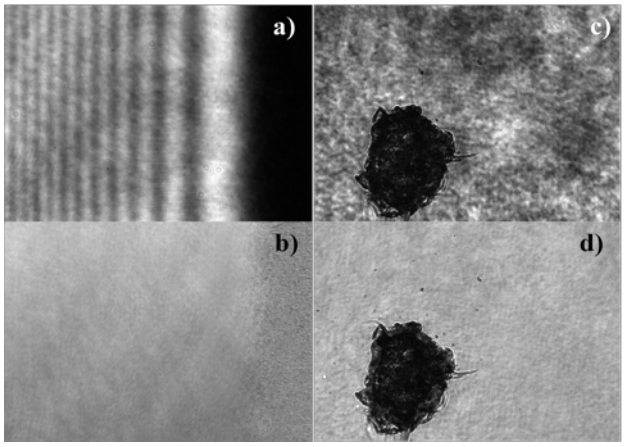

Figure 2. Demonstration of the image normalization process using pixel-by-pixel division of the raw and reference images (i.e., from damage and pristine sites, respectively). a) S-V image before and b) after normalization. c) T-V image before and d) after normalization.

The images were captured using strobe-light illumination provided by a 532 nm (2ω), ~4.5 ns probe pulse (Litron Lasers, UK). The timing of the probe pulse output was controlled by an adjustable delay trigger in reference to the pump pulse, allowing for image acquisition at any time point covering the entire timeline of events during damage initiation or growth. The pump-probe pulse jitter was determined to be ~2 ns. However, the arrival of the pump and probe pulses were separately recorded for each measurement using a set of fast photodiodes and the peak-to-peak time delay was obtained with ~0.5 ns resolution using a 500 MHz oscilloscope.

To remove static inhomogeneous features in the image arising from non-uniformities in the spatial profile of the probe laser beam, all images were divided by a reference image of a pristine site with no damage. Figure 2 shows examples of removal of such artifacts via image processing. In particular, Figs. 2a-b illustrate a raw transient image at 0 ns delay and the same image after normalization in the side-illumination mode. As a result, the interference fringes caused by the sample surface are largely removed. Similarly, in Figs. 2c-d the background non-uniformities in a static transmission image are likewise removed.

Typical images obtained with the basic system configuration of Fig. 1 are shown in Fig 3. Figure 3a shows an S-V image at 25 ns delay after exposure to the damage pulse. At least two shock fronts traveling through the air are visible which appear to originate from different points on the surface. However, no material motion is observed in this early delay time image. Figure 3b displays an S-V image taken at 400 ns delay. A jet of particles is visible originating from the surface and traveling through the air. Particles near the surface are close together and in focus while those further downstream are more spread out and some are out of focus. The diameters of the observed particles are around 1-10 μm. Also visible is the shock front traveling through the air with several particles ahead (downstream) of this front.

For estimating ejecta kinetics from the S-V images, it is necessary to precisely locate the surface of the sample, i.e. the origin of ejected particles. To locate the surface, images of the damaged surface were acquired with the S-V microscope after first blocking the S-V beam path, thus imaging the photons from the T-V beam path that were scattered by the damage site. An example is shown in Fig. 3c, where multiple scattering locations corresponding to multiple damage sites are visible as a series of vertically-oriented bright elongated spots on the right hand side of the image. Using this method, the location of the sample exit surface in the S-V images can be determined.

Figures 3d-e display images of a damage site captured by the T-V camera at two different points in time. Specifically, Fig. 3d shows the transient transmission image of a damage initiation site at 7 ns delay, while the final crater several seconds later is shown in Fig. 3e. These images show a difference in crater dimensions, revealing that the crater is

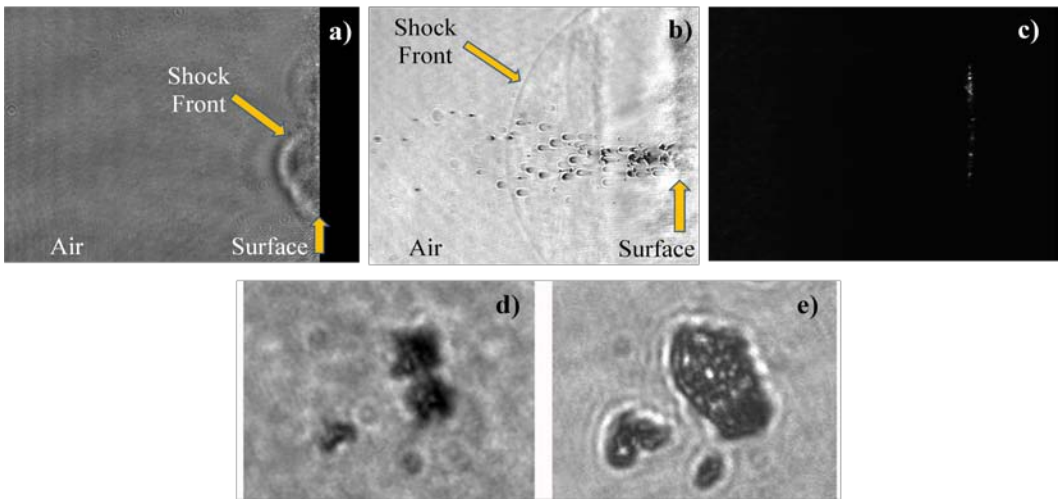

Figure 3. Typical images using simultaneous S-V and T-V imaging configurations. S-V images: a) at 25 ns delay, b) at 400 ns delay. c) Post-damage image captured by S-V microscope after blocking S-V beam and illuminating only with T-V beam. Transmission images at d) transient (7 ns delay) and e) final states of the same damage site.

evolving over this time scale. Distinct initiation sites appear to form initially but grow to the point where some of them finally coalesce.

The basic system configuration of Fig. 1 provides simultaneous S-V and T-V shadowgraphic imaging of the same event. S-V illumination permits the probing of a number of key processes, namely the kinetics of material cluster ejection, crater growth into the material, and near-surface phenomena prior to ejection (such as swelling and shock front generation). Material clusters appear as dark features because the probing beam is scattered and/or absorbed at these locations. This shadowgraphy mode provides a snapshot of their location and spatial characteristics during exposure to the probe pulse. The shock front in the air side is also visible because of the modulation it creates in the refractive index. With this system, average speeds of the particles and shock fronts can be estimated from the delay time of the probe pulse and distance traveled, assuming that the process started upon the damage pulse arrival (delay = 0 s).

T-V images provide views of the lateral expansion of the crater. As the absorption and scattering properties of the host material change in response to the laser energy deposition, the damage site appears as a dark object. Absorption dynamics can be measured when comparing an image in the transient state (during which the material is still undergoing modifications due to gradients in the local temperatures and pressures) to that in the final state (which represents the classical damage pit observed following a damage event). For example, the absorbing regions in Figs. 3d are observed to continue to grow laterally for about 25 ns. I. Information obtained via simultaneous transmission and side-view imaging makes possible the correlation between changes in lateral dimensions and with particle ejection, material swelling, and shock wave generation. Moreover, for resolving the early dynamic events as well as the ejection time of the particles, it is critical to accurately determine the location of the surface and employ the highest possible spatial resolution.

2.3 Dark-field configuration optimized for detecting early material motion

The results shown in Fig. 3a and 3d indicate that material changes occurring at earlier times are only partially visualized due to the obscuration in the S-V beam caused by the shock front. Thus a different configuration capable of better detecting early material motion is required.

In general, the ability of dark-field microscopy to detect small isolated particles is superior to that of bright-field microscopy. For this reason, we modified the previous configuration to employ an arrangement equivalent to dark-field microscopy. This was achieved by removing the beam-splitter and re-arranging the mirrors so as to direct the probe beam onto the exit surface location exposed to the pump pulse from the same direction used for image formation (photons detected by the S-V camera must undergo back-scattering) with the probe pulse incident at ~30 degrees with respect to the sample's exit surface. In this arrangement, transient images of damage site formation were recorded by the

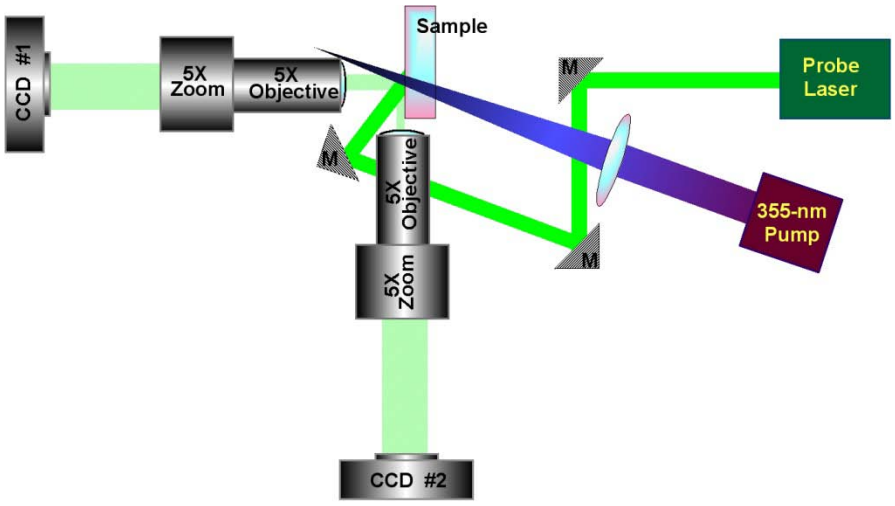

Figure 4. Pump- probe backscattering imaging configuration.

T-V CCD (#1) and S-V CCD (#2) as shown in Fig. 4. Material motion or ejection become visible by light directly scattered from the material (dark-field) rather than as a result of light obscuration (bright-field). All other laser damage and imaging parameters remained the same as in the basic system configuration shown in Fig. 1.

Figure 5 compares images acquired in the S-V shadowgraphy (bright-field) mode described in section 2.2 to those acquired using backscattering (dark-field) mode at the same delay times. These images are from different but similar damage events. Figures 5a-b show images acquired at 300 ns delay, where both images capture the particle ejection process. However, the advantage offered using the backscattering geometry is apparent in the images captured at early delay times. As an example, at 25 ns delay time, only the shock front is visible in the shadowgraphy mode (Fig. 5c), whereas material motion located behind the shock front is observable in the backscattering configuration (Fig. 5d).

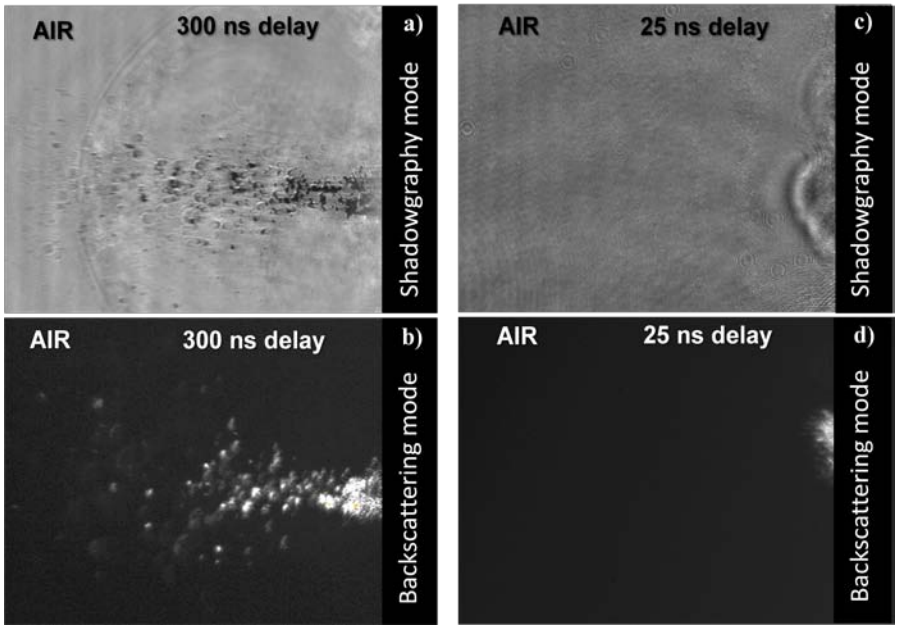

Figure 5. Images obtained by the S-V microscope using the shadowgraphy and backscattering modes at delay times of 300 ns [(a)-(b)] and 25 ns [(c)-(d)], respectively. Images are not from the same event and are intended to enable comparison of similar events using these different imaging modes.

The images suggest that a swelling of the surface precedes the ejection of individual particles capturing a critical part of the early material response to localized energy deposition.

Although shadowgraphic imaging can provide a wealth of information, the backscattering imaging configuration provides better sensitivity in detecting early material motion near the surface. This configuration is inherently sensitive to detecting small isolated particles and permits usage of the detector's full dynamic range. Similar to the S-V configuration, the backscattering configuration shows a jet of ejected material clusters. While not able to detect the shock front in the backscattering mode, this mode has the advantage that it is sensitive to early material response behind the expanding shock front. On the other hand, coherent artifacts like laser speckle can influence the quality of backscattering images which are largely absent in shadowgraphy. This configuration should also be able to detect concentrations of particles smaller than the resolution limit of the system (nano-particles) which will appear as "light scattering clouds."

2.4 Dual-probe configuration optimized for determining ejecta properties

The previous two system configurations are able to capture material motion and shock propagation spanning the entire timeline of an exit-surface damage event. These configurations can only capture one transient image per each distinct event. However, information on shock wave and particle trajectory can be more accurately retrieved by imaging the same event at multiple time points, especially when time-dependent motion parameters are involved (i.e., acceleration or deceleration). Therefore, an additional experimental configuration was implemented to better address these issues.

A configuration which adds the capability of capturing two transient images at different delay times per damage event is shown in Fig. 6. The basic system was expanded to include a second 532-nm probe laser whose pulse was delayed with respect to that of the first probe. To differentiate the images from each probe, we utilized a polarization filtering method in which the output polarizations of the two probe beams were set to be orthogonal to each other (i.e., vertical and horizontal). The two beams were then combined into a single beam path using a polarizing beam-splitter. A non-polarizing cube beam splitter was then used to separate the dual-probe beam into two paths to illuminate the damage site with the same geometry as the basic system (Fig. 1). In this manner, the image formed by the S-V microscope is a composite image of the damage site formed by the two probes delayed in time. A polarizing beam-splitter located behind the microscope's image-forming optics separates the two orthogonal polarization image components and directs them to separate CCD cameras. The time delays between the two probe pulses used for these experiments ranged from 100 to 500 ns.

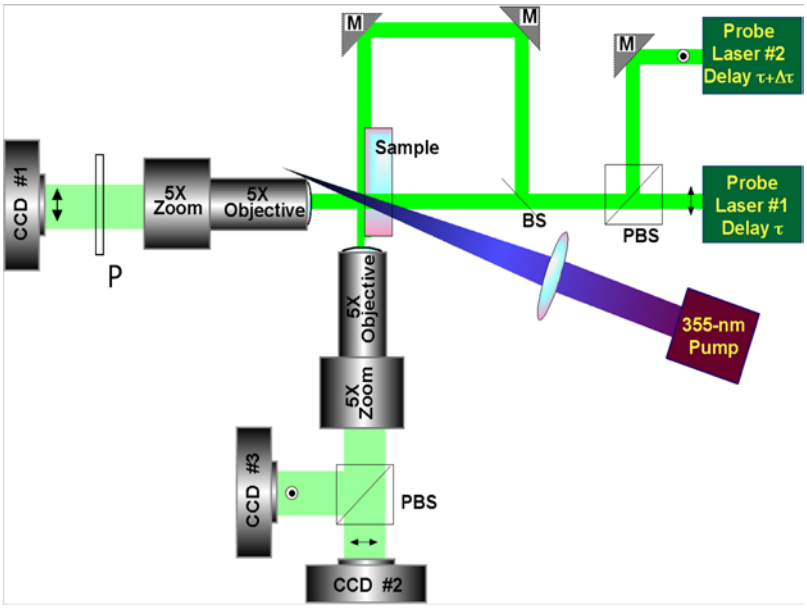

Figure 6. Pump- dual probe imaging configuration for S-V multi-image acquisition of the same damage event at different delay times.

For calibration and image co-registration between the two S-V cameras, probe 2 was turned off and a quarter-waveplate inserted into the probe 1 path to provide illumination of the damage site with circular polarization. This polarization state of the illuminating pulse enabled the acquisition of transient or static images with both CCD cameras by splitting the same image into two polarization components. Subsequently, the position of the cameras was adjusted so that both cameras provided exactly the same magnification, and the location of the surface was determined for each CCD.

Following this calibration process, we were able to accurately quantify the distance traveled by individual particles or shock fronts from their location in the two images captured at different delay times (i.e., dual probe imaging) . As a typical example, Fig. 7a shows particle ejecta at 2 μs delay, while Fig. 7b shows an image of the same event 500 ns later (at 2.5 μsec delay) when the particles have traveled further from the surface. The relative positions of the particles do not change for the most part, so most particles can be easily identified. in both images. In addition to translational motion, many particles can be seen to exhibit rotational motion. For example, the particles denoted as 1-6 in Fig. 7 exhibit different projected dimensions at the two time points, thus revealing their 3-dimensional shape.

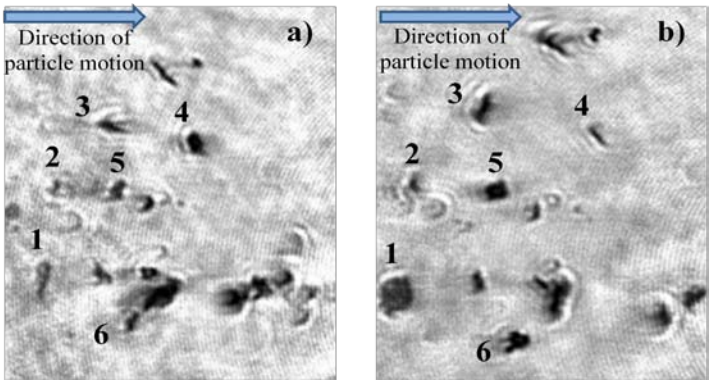

Figure 7. a) Side-view image at pump-probe delay of 2 μs. b) Image of same event 500 ns later. Five particles are identified for comparison.

While only the average dynamic properties of ejected particles are inferable based on single probe imaging, the dual-probe configuration directly measures the average speed of the ejected particles during the time interval between probe 1 and probe 2. This method also provides evidence that particles may have accelerated (for example when crossing the shock front) or decelerated along their trajectory from the surface. In addition to translational kinetic energy, comparison of the two images from this dual probe setup yields information on rotational motion and shape of the ejecta. With this system we are also able to estimate the ejection time of the particles observed in the images captured at different delay times. Preliminary results indicate that the ejection time can be as long as 20 μs after the arrival of the pump pulse.

2.5 Additional configurations

The basic system shown in Fig. 1 was additionally employed with other minor modifications. In the first modification, the 5 ns pulse probe laser was replaced by a laser with shorter pulse length of about 160 ps. This was necessitated by the high speed of some of the key observed parameters of the damage event. Specifically, the speed of the shock front in the material is on the order of the speed of sound and thus the ~4.5 ns probe pulse could only provide spatial resolution on the order of 30 μm. Similar limitations in the spatial resolution were observed for the case of shock fronts in air and the early motion of the surface and fast ejected particles. With the use of the 160 ps probe laser, these shortcomings were resolved and the spatial resolution of the dynamic features observed in the images was reduced to that of the static spatial resolution of the microscope (~1 μm). In the second modification, the S-V beam was translated to illuminate the sub-surface, bulk material to image the formation of the crater and its depth dimensions (as opposed to its lateral expansion, as seen in Figs. 3d-e). A final modification involved the use of the dual polarization imaging method using a single polarized probe. In this arrangement, the parallel polarization image (with respect to the polarization of the probe beam) provides the conventional shadowgraphic image while the perpendicular polarization image provides a map of the locations where stress fields induce a rotation of the polarization state of the probe beam. This approach is particularly useful in capturing the kinetics of the shock wave in the bulk of the material and the residual stress fields.

3. DISCUSSION

The material response to laser damage is multi-faceted, consisting of transient material absorption, generation of extreme temperatures and pressures over a microscopic volume, material motion, particle ejection, crater formation and growth, and generation of shock fronts. Although it is not the intention of this work to provide a detailed description of the experimental observations, the preliminary findings regarding rear surface damage in fused silica optical elements using the 7-ns FWHM, 355 nm laser pulses can be summarized as the following:

- During the laser pulse, the material reaches a critical energy density and the explosive process begins.
- During the later part of laser pulse, the host material appears to become absorptive and the absorptive region reaches about 50% of the final size of the damage site. The onset of material swelling on the surface is observed.
- From the end of the pulse to about 25 ns delay, the absorptive region continues to expand while surface swelling continues, leading to formation of a bulge on the surface.
- Between 25 and 100 ns delay, clusters of material with diameters of 1-4 μm and speeds of 1-3 km/sec are ejected from the bulge. The bulge starts disintegrating into smaller pieces that begin to move away from the surface.
- Between 100 and 2000 ns delay, a jet of nearly spherical or irregularly shaped clusters is formed with diameters between 1-25 μm. Ejection of material at later times includes flakes and chips with diameters up to 50 μm or larger.
- Beyond 2 μs delay, the ejection of material clusters continues while the ejecta speed continues to decrease to about 10 m/sec. Termination of the ejection process appears to take place at ~4 μs delay for damage initiation and at ~20 μs delay for damage growth.

The results also are strongly suggestive that damage initiation and growth evolve in the same manner but with two characteristic differences: a) the duration of the material ejection process, as discussed above and b) the speed of the shock front in the air, which is higher for damage growth, indicative of a higher energy deposition event.

4. CONCLUSIONS

In this work, we have presented a versatile time-resolved microscope system to obtain information on the dynamic behavior of the material during initiation and growth through the entire damage timeline. Various configurations of a single system are described such as simultaneous side-view and transmission-view imaging of distinct events, single and dual probe imaging of the same event at multiple time points, backscattering imaging to visualize the onset of material motion at early delays, and high resolution imaging to better resolve dynamic events. Each configuration is designed to best address different aspects of the damage timeline.

ACKNOWLEDGEMENTS

This work was performed under the auspices of the U.S. Department of Energy by Lawrence Livermore National Laboratory under Contract DE-AC52-07NA27344.

REFERENCES

[1] Norton, M. A., Hrubresh, L. W., Wu, Z. L., Donohue, E. E., Feit, M. D., Kozlowski, M. R., Milam, D., Neeb, K. P., Molander, W. A., Rubenchik, A. M., Sell, W. D., and Wegner, P., "Growth of laser initiated damage in fused silica at 351 nm," Proc. SPIE 4347, 468-468 (2001).

[2] Razè, G., Morchain, J. –M., Loiseau, M., Lamaignère, L., Josse, M., and Bercegol, H., "Parametric study of the growth of damage sites on the rear surface of fused silica windows," Proc. SPIE 4932, 127-135 (2003).

[3] Norton, M. A., Adams, J. J., Carr, C. W., Donohue, E. E., Feit, M. D., Hackel, R. P., Hollingsworth, W. G., Jarboe, J. A., Matthews, M. J., Rubenchik, A. M., and Spaeth, M. L., "Growth of laser damage in fused silica: diameter to depth ratio," Proc. SPIE 6720, 67200H (2007).

[4] Carr, C. W., Trenholme, J. B., and Spaeth, M. L., “Effect of temporal pulse shape on optical damage,” Appl. Phys. Lett. 90(4), 041110 (2007).
[5] Huang, W. Q., Han, W., Wang, F., Xiang, Y., Li, F. Q., Feng, B., Jing, F., Wei, X. F., Zheng, W. G., and Zhang, X. M., “Laser –induced damage growth on large aperture fused silica optical components at 351 nm,” Chin. Phys. Lett. 26(1), 017901 (2009).
[6] Kucheyev, S. O. and Demos, S. G., “Optical defects produced in fused silica during laser-induced breakdown,” Appl. Phys. Lett. 82(19), 3230-3232 (2003).
[7] Wong, J., Ferriera, J. L., Lindsey, E. F., Haupt, D. L., Hutcheon, I. D., and Kinney, J. H., “Morphology and microstructure in fused silica induced by high fluence ultraviolet 3ω (355 nm) laser pulses,” J. Non-Cryst. Solids 352(3), 255-272 (2006).
[8] Demos, S. G., Staggs, M., Minoshima, K., and Fujimoto, J., “Characterization of laser induced damage sites in optical components” Opt. Express 10(25), 1444-1450 (2002).
[9] Negres, R. A., Burke, M. W., DeMange, P. P., Sutton, S. B., Feit, M. D., and Demos, S. G., "Evaluation of UV absorption coefficient in laser-modified fused silica," Appl. Phys. 90(6), 061115 (2007).
[10] Russo, R. E., Mao, X. L., Liu, H. C., Yoo, J. H., and Mao, S. S., “Time-resolved plasma diagnostics and mass removal during single-pulse laser ablation,” Appl. Phys. A-Mater. 69, S887-S894 (1999).
[11] Carr, C. W., Radousky, H. B., Rubenchik, A. M., Feit, M .D., and Demos, S. G., “Localized dynamics during laser-induced damage in optical materials,” Phys. Rev. Lett. 92(8), 087401 (2004).
[12] Negres, R. A., Feit, M. D., DeMange, P., Bude, J. D., and Demos, S. G., “Pump and probe damage testing for investigation of transient material modifications associated with laser damage in optical materials,” Proc. SPIE 6720, 672019-1-6 (2008).